Existence of Different Structural Intermediates on the Fibrillation Pathway of Human Serum Albumin

Josué Juárez, Pablo Taboada,* and Víctor Mosquera
Grupo de Física de Coloides y Polímeros, Departamento de Física de la Materia Condensada, Facultad de Física, Universidad de Santiago de Compostela, Santiago de Compostela, Spain

ABSTRACT The fibrillation propensity of the multidomain protein human serum albumin (HSA) was analyzed under different solution conditions. The aggregation kinetics, protein conformational changes upon self-assembly, and structure of the different intermediates on the fibrillation pathway were determined by means of thioflavin T (ThT) fluorescence and Congo Red absorbance; far- and near-ultraviolet circular dichroism; tryptophan fluorescence; Fourier transform infrared spectroscopy; x-ray diffraction; and transmission electron, scanning electron, atomic force, and microscopies. HSA fibrillation extends over several days of incubation without the presence of a lag phase, except for HSA samples incubated at acidic pH and room temperature in the absence of electrolyte. The absence of a lag phase occurs if the initial aggregation is a downhill process that does not require a highly organized and unstable nucleus. The fibrillation process is accompanied by a progressive increase in the β-sheet (up to 26%) and unordered conformation at the expense of α-helical conformation, as revealed by ThT fluorescence and circular dichroism and Fourier transform infrared spectroscopies, but changes in the secondary structure contents depend on solution conditions. These changes also involve the presence of different structural intermediates in the aggregation pathway, such as oligomeric clusters (globules), bead-like structures, and ring-shaped aggregates. We suggest that fibril formation may take place through the role of association-competent oligomeric intermediates, resulting in a kinetic pathway via clustering of these oligomeric species to yield protofibrils and then fibrils. The resultant fibrils are elongated but curly, and differ in length depending on solution conditions. Under acidic conditions, circular fibrils are commonly observed if the fibrils are sufficiently flexible and long enough for the ends to find themselves regularly in close proximity to each other. These fibrils can be formed by an antiparallel arrangement of β-strands forming the β-sheet structure of the HSA fibrils as the most probable configuration. Very long incubation times lead to a more complex morphological variability of amyloid mature fibrils (i.e., long straight fibrils, flat-ribbon structures, laterally connected fibers, etc.). We also observed that mature straight fibrils can also grow by protein oligomers tending to align within the immediate vicinity of the fibers. This filament + monomers/oligomers scenario is an alternative pathway to the otherwise dominant filament + filament manner of the protein fibril's lateral growth. Conformational preferences for a certain pathway to become active may exist, and the influence of environmental conditions such as pH, temperature, and salt must be considered.

INTRODUCTION

β-Sheet-based assemblies have attracted much interest from multidisciplinary researchers because of their association with a variety of diseases and their emerging potential in material science and biotechnology (1,2). Protein misfolding and self-assembly into highly ordered β-sheet-rich fibrillar assemblies known as amyloid fibrils are common features of a growing class of systemic and neurodegenerative diseases, including Alzheimer's, Parkinson's, and Huntington's diseases; senile systemic amyloidoses; type II diabetes (3,4); and many others. The ability to fibrillate is independent of the original native structure of the protein, whose amino acid sequence primarily appears to play a key role in terms of filament arrangement (5), fibrillation kinetics (6), and overall yield and stability of the fibrils (7,8). Fibrillation originates under conditions in which proteins are partially destabilized or completely unfolded (9), and the formation of the amyloid fibrils reflects an alternative to the native packing conformational struggle of a polypeptide chain to 1), reduce its surface-accessible area; 2), saturate hydrogen bonding; and 3), reach an alternative ''nonnative'' global free energy minimum (10). Therefore, investigators have emphasized understanding and inhibiting amyloid formation more so than amyloid dissociation and clearance. Although the stability of β-sheet-rich amyloid fibrils against proteases, acids, and chemical denaturants has been shown, increasing evidence from human (11) and in vitro studies indicates that a dynamic structure exists within amyloid fibrils and suggests that the process of amyloid formation is reversible (12). These findings, along with the fact that strategies aimed at stabilizing amyloid fibrils and/or accelerating their clearance seem to reverse the disease phenotype (13,14), suggest that a detailed understanding of the formation, stability, and dynamic behavior of amyloid fibrils is critically important to the development of therapeutic strategies for amyloid diseases. Thus, the reversible untangling of amyloid architecture and intrafibrillar packing of the β-pleated sheets is a key issue to consider in designing inhibitors of fibrillar growth (15), and insights into the fibrillar assembly mechanisms may help elucidate the etiology of the ''prion diseases'', provided that the subtle structural differences underlying the puzzling phenomenon of ''prion strains'' can be understood (16).

Submitted September 30, 2008, and accepted for publication December 1, 2008.

*Correspondence: pablo.taboada@usc.es

Editor: Ruth Nussinov.

0006-3495/09/03/2353/18 $2.00

doi: 10.1016/j.bpj.2008.12.3901

Because of the physiological importance of human serum albumin (HSA) as a carrier protein and blood pressure regulator, and its propensity to easily aggregate in vitro, HSA has become a good model for protein aggregation studies. Moreover, as the phenomenon of protein aggregation appears to reflect certain generic ''polymeric'' features of proteins (17), studying mechanisms of protein aggregation in model systems is extremely useful for gaining a better understanding of the molecular mechanisms of disease-associated amyloidogenesis.

Under physiological conditions, HSA consists of 585 amino acids in a single polypeptide chain, with a globular structure composed of three main domains that are loosely joined together through physical forces and six subdomains that are wrapped by disulfide bonds. The protein contains 17 disulfide bridges and one free SH group, which facilitates dimerization and also influences higher-order association. Native HSA lacks any properties that suggest a predisposition to form amyloid fibrils, since most of its sequence (>60%) is arranged in an α-helix structure, with subsequent tightening of its structure through intramolecular interactions such as hydrogen bonds. Therefore, serum albumin aggregation is promoted under conditions that favor partly destabilized monomers and dimers, such as low pH, high temperature, and the presence of chemical denaturants (18). In a recent report (19), we showed that partially destabilized HSA molecules form amyloid-like fibrils and other types of aggregates under different solution conditions. These fibrils feature the structural characteristics of amyloids: x-ray diffraction (XRD) patterns, affinity to Congo Red (CR) and thioflavin T (ThT), birefringence, and high stability. We now extend that previous work to shed further light on the kinetics and hierarchical assembly of HSA fibril formation, linking the morphological structural transitions of aggregated protein intermediates to conformational events on protein structure as analyzed by means of different biophysical and spectroscopic methods. In this way, we present a systematic investigation of the relationship between protein conformation and the amyloid-like self-assembly pathway for HSA under different solution conditions. To this end, we incubated the protein under different thermal and solvent conditions and analyzed the protein conformation changes upon incubation. We additionally imaged different structural intermediates on the HSA fibrillation pathway depending on solution conditions. In this way, we sought to uncover the structural features underlying the formation of possibly cytotoxic HSA assemblies.

MATERIALS AND METHODS

Materials

HSA (70024-90-7), CR, and ThT were obtained from Sigma (St. Louis, MO) and used as received. All other chemicals were of the highest purity available.

Preparation of HSA solutions

Protein was used after further purification by liquid chromatography using a Superdex 75 column equilibrated with 0.01 M phosphate. Experiments were carried out using double-distilled, deionized, and degassed water. The buffer solutions used were glycine + HCl (I = 0.01 M) for pH 3.0, and sodium monophosphate-sodium diphosphate for pH 7.4 (I = 0.01 M), respectively. HSA was dissolved in each buffer solution to a final concentration of typically 20 mg/mL and dialyzed extensively against the proper buffer. Protein concentration was determined spectrophotometrically using a molar absorption coefficient of 35,219 M^{-1} cm^{-1} at 280 nm (20). Before incubation, the solution was filtered through a 0.2 μm filter into sterile test tubes. Samples were incubated at a specified temperature in a refluxed reactor. Samples were taken out at intervals and stored on ice before addition of CR or ThT.

Seeding solutions

To test whether seeding with preformed aggregates increases the rate of HSA aggregation under the different conditions in which fibrils are formed, a protein solution was incubated for 24 h and an aliquot that corresponded to 10% (w/w) of the total protein concentration was then added to a fresh protein solution.

CR binding

Changes in the absorbance of CR dye produced by binding onto HSA were measured in an ultraviolet-visible spectrophotometer (DU series 640; Beckman Coulter, Fullerton, CA) operating at 190–1100 nm. All measurements were made in the wavelength range of 220–500 nm in matched quartz cuvettes. Protein solutions were diluted 20- to 200-fold into a buffer solution with 5 μM of CR (Acros Organics, Geel, Belgium). Spectra in the presence of the dye were compared with those of the buffer containing CR in the absence of protein and also with those corresponding to the protein solution without dye.

ThT spectroscopy

Protein and ThT were dissolved in the proper buffer at a final protein/dye molar ratio of 50:1. Samples were continuously stirred during measurements. Fluorescence was measured in a Cary Eclipse fluorescence spectrophotometer equipped with a temperature control device and a multicell sample holder (Varian Instruments, Palo Alto, CA). Excitation and emission wavelengths were 450 and 482 nm, respectively. All intensities were background-corrected for the ThT fluorescence in the respective solvent without the protein.

Protein fluorescence

To examine the conformational variations around the Tryp residue of HSA, fluorescence emission spectra were recorded with a Cary Eclipse fluorescence spectrophotometer equipped with a temperature control device and a multicell sample holder (Varian Instruments). HSA samples were excited at 295 nm, which provides no excitation of tyrosine residues and, therefore does not cause emission or energy transfer to the lone side chain. Slit widths were typically 5 nm.

Circular dichroism

Far- and near-ultraviolet (UV) circular dichroism (CD) spectra were obtained using a JASCO-715 automatic recording spectropolarimeter (Jasco, Tokyo, Japan) with a JASCO PTC-343 Peltier-type thermostated cell holder. Quartz cuvettes with 0.2 cm pathlength were used. CD spectra were obtained from aliquots withdrawn from the aggregation mixtures at the indicated conditions and recorded between 195 and 300 nm at 25°C. The mean residue ellipticity θ (deg cm^2 $dmol^{-1}$) was calculated from the formula:

$\theta = (\theta_{obs}/10)(MRM/lc)$, where θ_{obs} is the observed ellipticity in deg, MRM is the mean residue molecular mass, l is the optical pathlength (in centimeters), and c is the protein concentration (in g mL^{-1}). To calculate the composition of the secondary structure of the protein, SELCON3, CONTIN, and DSST programs were used to analyze far-UV CD spectra. Final results were assumed when data generated from all programs showed convergence (21).

XRD

XRD experiments were carried out using a Siemens D5005 rotating anode x-ray generator. Twin Göbel mirrors were used to produce a well-collimated beam of CuKα radiation ($\lambda = 1.5418$ A). Samples were put into capillary with a diameter of 0.5 mm. X-ray diffraction patterns were recorded with an imaging plate detector (AXS F.Nr. J2-394).

Fourier transform infrared spectroscopy

Fourier transform infrared (FTIR) spectra of HSA in aqueous solutions were determined by using an FTIR spectrometer (model IFS-66v; Bruker) equipped with a horizontal ZnS ATR accessory. The spectra were obtained at a resolution of 2 cm^{-1} and generally 200 scans were accumulated to obtain a reasonable signal/noise ratio. Solvent spectra were also examined under the same accessory and instrument conditions. Each different sample spectrum was obtained by digitally subtracting the solvent spectrum from the corresponding sample spectrum. Each sample solution was repeated three times to ensure reproducibility and averaged to produce a single spectrum.

Transmission electron microscopy

For transmission electron microscopy (TEM), suspensions of HSA were applied to carbon-coated copper grids, blotted, washed, negatively stained with 2% (w/v) of phosphotungstic acid, air dried, and then examined with a Phillips CM-12 transmission electron microscope operating at an accelerating voltage of 120 kV. Samples were diluted 20- to 200-fold when necessary before deposition on the grids.

Scanning electron microscopy

Suspensions of HSA were applied to glass-coated stainless-steel grids, blotted, washed, air dried, and then examined with an LEO-435VP scanning electron microscope (Leica Microsystems GmbH, Wetlar, Germany) operating at an accelerating voltage of 30 kV. Samples were diluted 20- to 200-fold when necessary before deposition on the grids. Microanalysis of the scanning electron microscopy (SEM) samples was also performed to avoid the presence of impurities.

Atomic force microscopy

Atomic force microscopy (AFM) images were recorded in tapping mode by using a multimode SPM microscope equipped with a Nanoscope IIIa controller from Digital Instruments (Santa Barbara, CA). The microscope was coupled to an AS-12 resp. E-scanner and an Extender Electronics Module EX-II, which allows acquisition of phase images. The AFM probes were typically silicon SPM sensors (NCHR Nanosensors, Neuchatel, Switzerland). Immediately after incubation, the protein samples were diluted 20–400 times onto freshly cleaved muscovite mica (Sigma) attached to a magnetic steel disc that served as the sample holder. The abrupt dilution of the samples immediately quenched the concentration-dependent aggregation process. The AFM samples were dried on air or under nitrogen flow when required. Control samples (freshly cleaved mica, and mica and buffer solution) were also investigated with AFM to exclude possible artifacts. Height and phase-shift data were collected in the trace and the respective retrace direction of the raster. The scan rate was tuned proportionally to the area scanned and was kept within the 0.35–2 Hz range.

RESULTS

It is generally accepted that amyloid formation usually is a result of misfolded and partially unfolded states acting in competition with the normal folding pathways (22–24). The HSA molecule is known to undergo several well-organized changes during its conformation, usually under nonphysiological conditions, as follows:

1. The N-F transition between pH 5.0 and 3.5 involves the unfolding and separation of domain III without significantly affecting the rest of the protein molecule (25,26). The F form is characterized by a dramatic increase in viscosity, lower solubility, and a significant loss of helical content.
2. The F-E transition occurs between pH 3.5 and 1.2, and is accompanied by a further protein expansion with a loss of the intradomain helices of domain I. In addition, the E form involves an increase in protein intrinsic viscosity and a rise in the hydrodynamic axial ratio from ~4 to 9 (27).
3. The N-B transition occurs between pH 7.0 and 9.0, with a slight reduction in helical content affecting the two interdomain helices and a small increase in sheet structure (28).
4. In the presence of denaturant agents, such as urea, HSA shows a two-step, three-state transition with an intermediate (I) characterized by unfolding of the domain III and partial but significant loss of native conformation of domain I (29).

Therefore, an easy way to obtain at least partially denaturated states is to induce a temperature-induced or solvent-induced protein denaturation process through incubation. Thus, HSA was subjected to conditions previously found to be effective for protein aggregation, in particular those that induce amyloid-like fibril formation (19,30). HSA solutions were incubated at a concentration of 20 mg/mL in 0.01 M sodium phosphate buffer, pH 7.4, or 0.01 M glycine buffer, pH 3.0, in the presence of 0 or 50 mM of added NaCl at 25°C or 65°C for 15 days. We chose 65°C as the incubation temperature because HSA temperature-induced denaturation takes place through a two-state transition with a first melting temperature, T_m, of ~56°C and a second T_m of ~62°C (31,32) as a consequence of the sequential unfolding of the different domains of the protein, in particular, the IIA and IIIA subdomains. Moreover, as the pH becomes more acidic, T_m becomes lower. We confirmed these melting temperatures under our solution conditions by fluorescence spectroscopy, and the results were in close agreement with previously reported data (see Table S1 in the Supporting Material). Therefore, it can be inferred that aggregation is unfavorable below 65°C because protein folding competes with and suppresses amyloid formation. It is known that hydrogen bonding is weakened as temperature rises, but the hydrophobic interaction becomes strengthened (33). As the heating process continues, some of the cooperative hydrogen bonds

that stabilized helical structure begin to break and expose hydrophobic groups to the solvent, partially unfolding the protein structure, which favors aggregation.

Physiological conditions: kinetics and amyloid self-assembly of HSA

The propensity of protein solutions to form amyloid-like aggregates under physiological conditions was assessed by means of ThT fluorescence and CR absorbance measurements. These two dyes specifically bind to ordered β-sheet aggregates and, notably, to amyloid fibrils (34,35). Both assays are necessary because positive ThT binding sometimes does not occur with certain amyloid fibril systems (36). Before incubation, native HSA does not display a capacity to bind ThT. When incubated at physiological pH and room temperature, the fluorescence emission intensity for the protein at 482 nm is negligible, suggesting that HSA does not form amyloid fibrils or other types of fluorescent aggregates under these conditions. When the temperature is raised to 65°C, a time-dependent increase in fluorescence is observed (Fig. 1, *a* and *b*). The kinetics of HSA involved the continuous rising of ThT fluorescence during the early periods of the incubation procedure, and exhibited no discernible lag phase until a quasi-plateau region was attained in the timescale analyzed. The addition of electrolyte favors a faster formation of amyloid fibrils as a consequence of the screening of electrostatic repulsions between protein molecules (37). In fact, a gel phase can be observed after 4 days of incubation, which denotes an enhanced development of fibril formation because cross-links can be formed more easily, resulting in a lower critical percolation concentration.

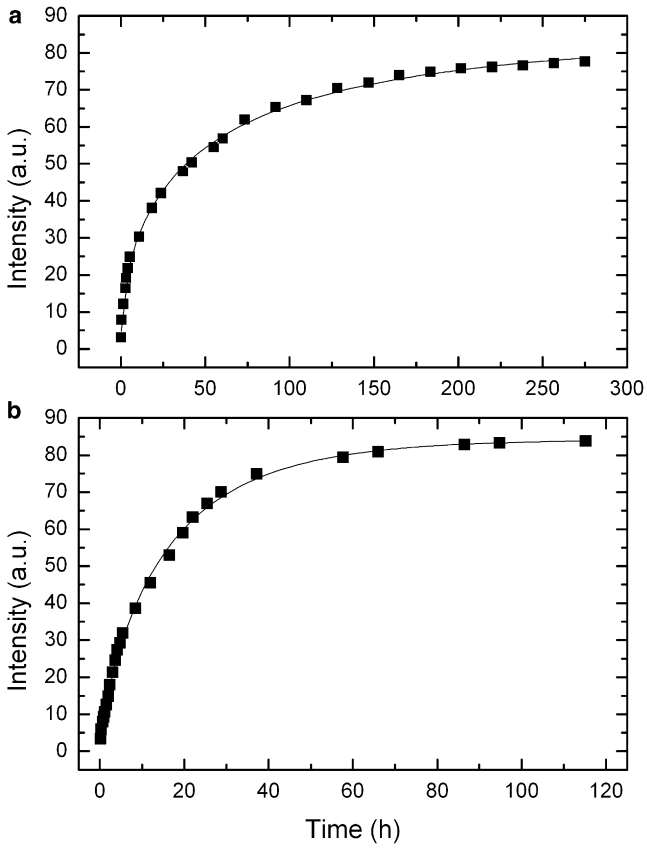

FIGURE 1 Time evolution of ThT fluorescence in HSA solutions incubated at 65°C at pH 7.4 in the (*a*) absence and (*b*) presence of 50 mM NaCl.

ThT fluorescence curves were fitted by means of nonlinear square curve-fitting to a stretched exponential function $F = F^{\infty} + \Delta F\exp(-[k_{sp}t]^n)$ to obtain information on the kinetics of amyloid formation. F, F^{∞}, and ΔF are the observed fluorescence intensity at time t, the final fluorescence intensity, and the fluorescence amplitude, respectively, and k_{sp} is the rate of spontaneous fibril formation. Although the interpretation of the parameters involved in this equation is not straightforward, these are useful for empiric descriptions of the complex reactions whose kinetics is not easily modeled (38,39). Values of k_{sp}, n, and ΔF determined in this way under the different conditions are shown in Table 1. Values of $n < 1$ indicated that the kinetics can be approximated to several exponential functions indicative of the existence of multiple events in the amyloid formation. Furthermore, larger k_{sp} values in the presence of electrolyte corroborate the more-efficient aggregation due to electrostatic screening under high ionic strength conditions.

CR absorption also corroborates the formation of amyloid fibrils, displaying a progressive red shift from 495 to ~530 nm of the differential absorption maximum at 65°C in both the absence and presence of added electrolyte, a typical feature of amyloid fibers (35). Since absorption of HSA alone after incubation contributes to only ~15% of the increase in CR absorption, the change in absorption is mainly caused by the formation of CR-binding species (see Fig. S1 in the Supporting Material).

Fibrillation is independent of seeding at physiological pH

Typical fibrillation processes involve a lag phase followed by a relatively rapid elongation phase that stabilizes when all

TABLE 1 Kinetic parameters of the self-assembly process of HSA solutions

	F^{∞}	ΔF	n	k_{sp} (h^{-1})
		pH 7.4		
65°C				
0 mM NaCl	85	83	0.56	0.019
50 mM NaCl	85	83	0.82	0.064
		pH 3.0		
25°C				
0 mM NaCl	10	8	1.34	0.007
50 mM Na Cl	13	11	1.57	0.007
65°C				
0 mM NaCl	8/30	6/22	1.25/3.6	0.144/0.005
50 mM NaCl	59	57	0.96	0.010

monomers have been incorporated into fibrils (40–42). In our case, the absence of a lag phase at pH 7.4 would suggest that nuclei are either formed very rapidly or the aggregation process we monitor is not a classical nucleation-based fibrillation. If nuclei consist of more than one molecule, their formation will be reduced if the HSA concentration is lowered. Nevertheless, when the protein concentration was decreased to 0.5 and 2 mg/mL at 65°C, we did not observe the appearance of a lag phase (figure not shown). In addition, another feature that confirms a continuous fibrillation process without a nucleation step is the absence of any remarkable effect on the fluorescence curves when protein seeds were added to protein solutions followed by subsequent incubation (see Fig. S2). The aggregation rate during the growth phase was unchanged by the addition of preformed aggregates and followed apparent first-order kinetics. These characteristics suggest that aggregation does not require nucleation, i.e., each protein monomer association step is bimolecular and effectively irreversible, and there is no energy barrier to aggregate growth. As discussed in detail below, TEM pictures showed the formation of spherical oligomers after very short incubation times. This usually occurs by a mechanism of classical coagulation, or downhill polymerization (43), that does not require a nucleation step.

Structural changes upon aggregation at physiological conditions: secondary structure

To gain insight into the structural protein modifications upon formation of amyloid-like aggregates, we recorded CD, FTIR, and tryptophan (Tryp) fluorescence spectra. As a supplement to ThT and CR assays, which provide information only about the formation of fibrillar protein assemblies, far-UV CD and FTIR data reveal the overall protein secondary structural composition and their evolution to form amyloid-like or amorphous aggregates. On the other hand, near-UV CD and Tryp fluorescence data denote changes in protein tertiary structure (for the latter technique, particularly in domain II of HSA).

Fig. 2, *a* and *b*, show far-UV CD spectra of HSA at pH 7.4 at 25°C and 65°C. The spectra at room temperature in the absence of added salt show two minima—one at 208 and other at 222 nm—characteristic of helical structure, which remains unmodified upon incubation. When electrolyte is present, a small decrease in ellipticity, [θ], occurs as a consequence of small changes in protein structure originating from the formation of some amorphous aggregates in solution, as shown in Fig. 2 *a*. In contrast, when the temperature is raised to 65°C, the minimum at 222 nm progressively disappears and [θ] at 208 nm also strongly reduces (Fig. 2 *b*). This indicates that high-temperature conditions spawn intermediates that are clearly less helical than the starting conformations. This change in CD spectra suggests the increment of either β-sheet or loop structures, as discussed in detail further below. The intensity loss of the 222 nm band indicates that the increase in random coil/β-sheet conformations is accompanied by a reduction in the α-helical content of the protein structure. At longer incubation times in the absence of added salt in solution (~72 h), the CD spectrum resembles that typical of proteins with high proportions of β-sheet structure, which are characterized by a minimum at ~215–220 nm and small [θ] values as a consequence of the presence of amyloid-like aggregates in solution. On the other hand, no significant changes in far-UV CD spectra are observed when electrolyte is added to solutions, except that the characteristic features of β-sheet structure are present at earlier incubation times at elevated temperature. A larger decrease in [θ] is also detected as a consequence of the increased number and size of scattering objects in solution, which agrees with the formation of a fibrillar gel upon longer incubation times.

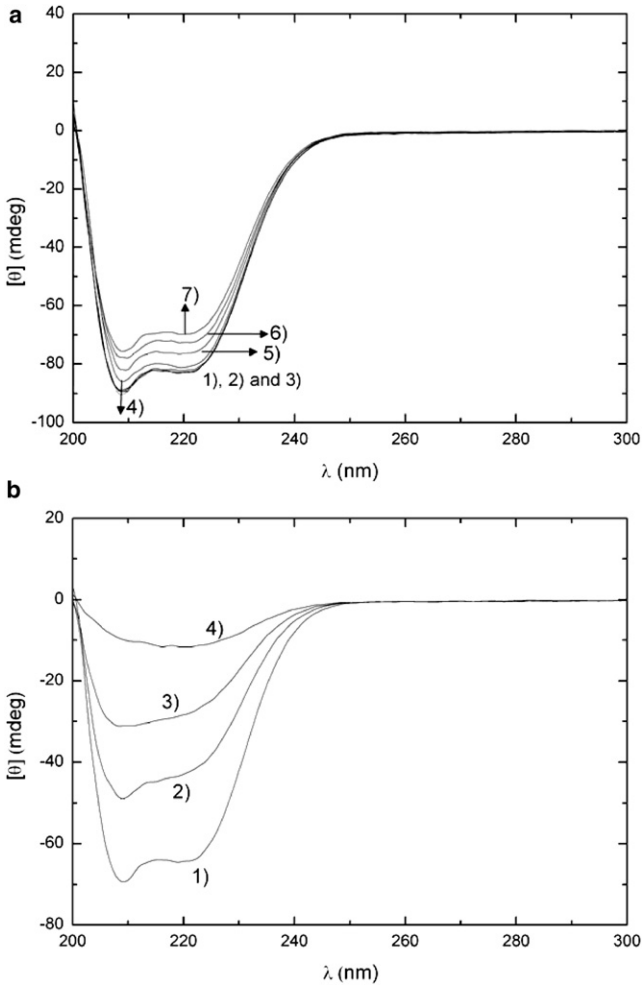

FIGURE 2 (*a*) Far-UV spectra of HSA solutions at 25°C in the presence of 50 mM NaCl at pH 7.4 at 1), 0 h; 2), 24 h; 3), 48 h; 4), 100 h; 5), 200 6), and 7), 250 h of incubation. (*b*) Far-UV spectra of HSA solutions at 65°C in the presence of 50 mM NaCl at 1), 0 h; 2), 12 h; 3), 24 h; and 4), 48 h of incubation.

Fig. 3 depicts the temporal evolution of the secondary structure composition as revealed by CD analysis (21). At pH 7.4 and room temperature, the initial α-helix content is ~59%, the β-sheet conformation is ~5%, the turn content

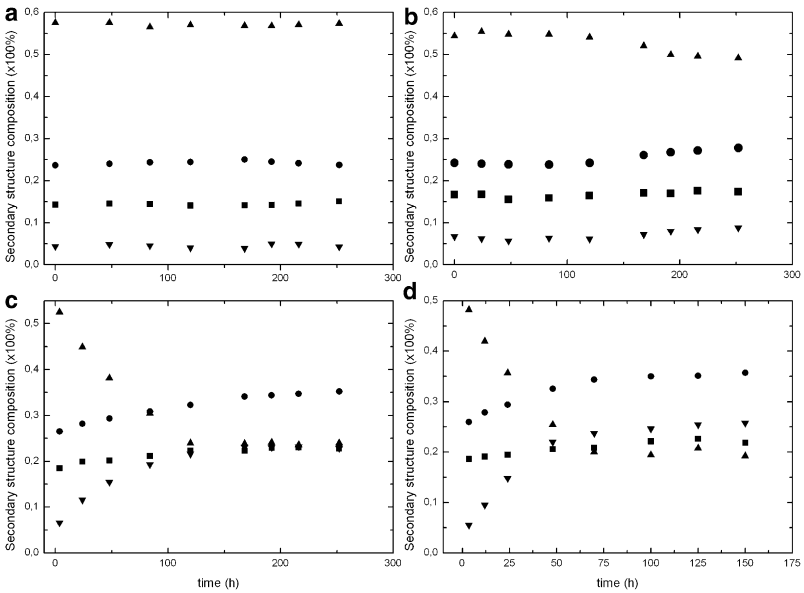

FIGURE 3 Time evolution of secondary structure compositions of HSA solutions at pH 7.4 at 25°C (*a* and *b*) or 65°C (*c* and *d*) in the absence and presence of 50 mM NaCl, respectively. (▲) α-helix, (■) β-turn, (●) unordered, and (▼) β-sheet conformations.

is ~13%, and the remaining random coil content is ~23%, in agreement with previous reports (25). In the presence of added electrolyte, no significant alterations in the structure compositions are observed upon incubation; the initial α-helix content is slightly reduced to ~55%, in contrast to a very small increase in turn and β-sheet conformations. After ~150 h of incubation, an additional slight decrease in α-helix is observed due to an enhancement of protein aggregation, i.e., the formation of a certain amount of protein aggregates is observed, which is a characteristic feature of globular proteins under high ionic strength conditions.

On the other hand, protein conformational compositions at 65°C after incubation indicate an increase in β-sheet conformation from ~5% to ~21% at the expense of the α-helix content (which diminishes from ~59% to ~20%) in the absence of electrolyte. This is also reflected by the decrease in the CD signal and the shift of the spectral minimum from 208 nm to longer wavelengths, as noted above. Coil and turn conformations also change through the incubation process, with values of ~27–34% and ~17–21%, respectively. The alteration in structure composition seems to be stronger when salt is added, due to electrostatic screening, which favors protein disruption and association by modifying the balance of interactions, with final β-sheet and α-helix contents of ~26% and ~19%, respectively (Fig. 3). Moreover, changes in secondary structure take place during the first part of the incubation process in both the absence (~90 h) and presence of electrolyte (~50 h), respectively, and occur more rapidly under the latter condition. At very long incubation times (>150 h) under high ionic strength conditions, the increased scattering from the fibrillar aggregates makes it difficult to estimate the secondary structure; thus, these results are not shown in Fig. 3.

FTIR spectra were recorded at the beginning and end of the incubation process by monitoring the observed changes in the shape and frequency of the amide I and II bands, and the results corroborated the CD data. Before incubation, two major absorption peaks in the spectral region of interest were observed: the amide I band at 1653 (1652) cm^{-1} and the amide II band at 1542 (1544) cm^{-1} in both the original and second derivative IR spectra, respectively. This indicates the predominant structural contribution of major α-helix and minor random coil structures, in agreement with CD data (44–46). For the amide I band (Fig. 4 *a*), a shoulder at ~1630 cm^{-1} can be also observed in the second derivative spectra that is related to intramolecular β-sheet structure. Additional peaks at ~1689 and 1514 cm^{-1} would correspond to β-turn and tyrosine absorption, respectively (45). All of these peaks were also observed in the presence of electrolyte at room temperature as

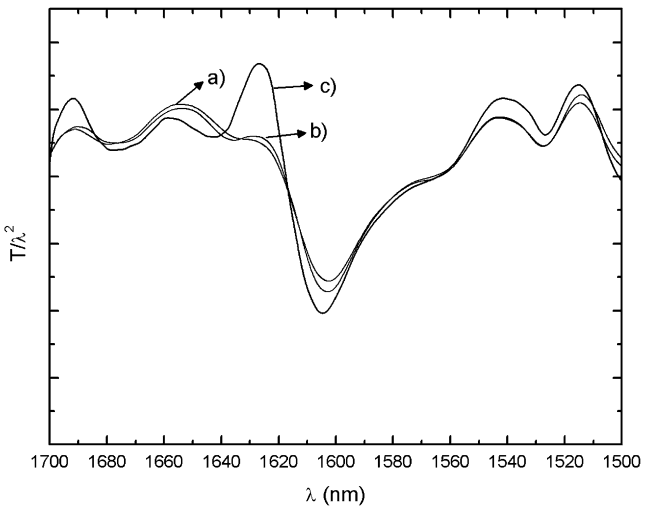

FIGURE 4 Second derivative of FTIR spectra at pH 7.4 of (*a*) native HSA at 25°C before incubation, (*b*) HSA at 25°C in the presence of 50 mM NaCl, and (*c*) HSA at 65°C in the absence of electrolyte.

incubation proceeded (Fig. 4 *b*), compatible with little changes in secondary structure composition, as noted above.

After incubation at 65°C, a red shift of the amide I band from 1652 to 1658 cm^{-1} and a blue shift of the amide II band to 1542 cm^{-1} in the second derivative spectrum are indicative of a certain increase of disordered structure, as revealed by far-UV CD (Fig. 4 *c*). The appearance of a well-defined peak around 1628 cm^{-1} (1626 cm^{-1} in the presence of added salt) points to a structural transformation from an intramolecular hydrogen-bonded β-sheet to an intermolecular hydrogen-bonded-β-sheet structure (47). The spectrum also shows a high-frequency component (~1692 cm^{-1}) that would suggest the presence of an antiparallel β-sheet (48). In addition, a little shoulder around 1534 cm^{-1} also was assigned to β-sheet after incubation at high temperature (49). The increase in the band associated with β-sheet in the FTIR spectra correlates well with the large changes in CD spectra. On the other hand, peak shifts are slightly more abrupt when electrolyte is present in solution because the aggregation is stronger (plot not shown). This leads to the formation of a fibrillar gel favored by the decrease in electrostatic repulsions and a change in the hydration layer surrounding the protein molecules that allows interfibrillar attachment.

Structural changes upon aggregation at physiological conditions: tertiary structure

At room temperature, the near-UV CD spectrum showed two minima at 262 and 268 nm and two shoulders around 275 and 285 nm, characteristic of disulphide and aromatic chromophores and the asymmetric environment of the latter (Fig. 5 *a*) (50). These features are significantly retained during incubation in the presence of electrolyte excess despite the formation of some amorphous aggregates in solution, as noted above (figure not shown). On the other hand, when the incubation temperature is raised to 65°C, important alterations in the near-UV CD spectra occur in both the absence and presence of electrolyte: ellipticity decreases, and the minima at 262 and 268 nm progressively disappear as incubation proceeds. In addition, a significant loss of fine structure detectable in the region of 270–295 nm also occurs. Nevertheless, these changes in near-UV CD data are less marked than in far-UV measurements because secondary structural changes are more sensitive to temperature than tertiary structural changes (51). These effects corroborate alterations in tertiary structure upon fibrillation conditions.

The behavior described by near-CD UV measurements is also supported by tryptophanyl fluorescence data. HSA has a single tryptophanyl residue, $Tryp^{214}$, located in domain II. A very small change in fluorescence emission occurs with incubation at room temperature in the presence of electrolyte, confirming the existence of little variations in tertiary structure, in agreement with previous data (not shown). In contrast, when the temperature is raised to 65°C, a 4 nm hypsochromic shift (from 341 to 337 nm) takes place accompanied by a reduction in fluorescence intensity: the domain II of HSA unfolds in such a way that the Trp^{214} residue of HSA located at the bottom of a 12 Å deep crevice (52) finds itself in a more hydrophobic environment (32). As incubation at elevated temperature proceeds, conversion of protein molecules to fibrils is accompanied by an additional burial of the Tryp residue, as indicated by the decrease of the Tryp fluorescence emission intensity (Fig. 5 *b*) and the further blue shift of the emission maximum from 337 to 333 nm (53). All of this points to the strong involvement of tertiary structure changes of domain II of HSA in the fibrillation mechanism. This change is enhanced and occurs more rapidly in the presence of added electrolyte, which confirms a larger structure alteration as a consequence of enhanced intermolecular interactions to give fibrillar assemblies. This also agrees with the increasing content of β-sheet conformation revealed by CD and FTIR measurements.

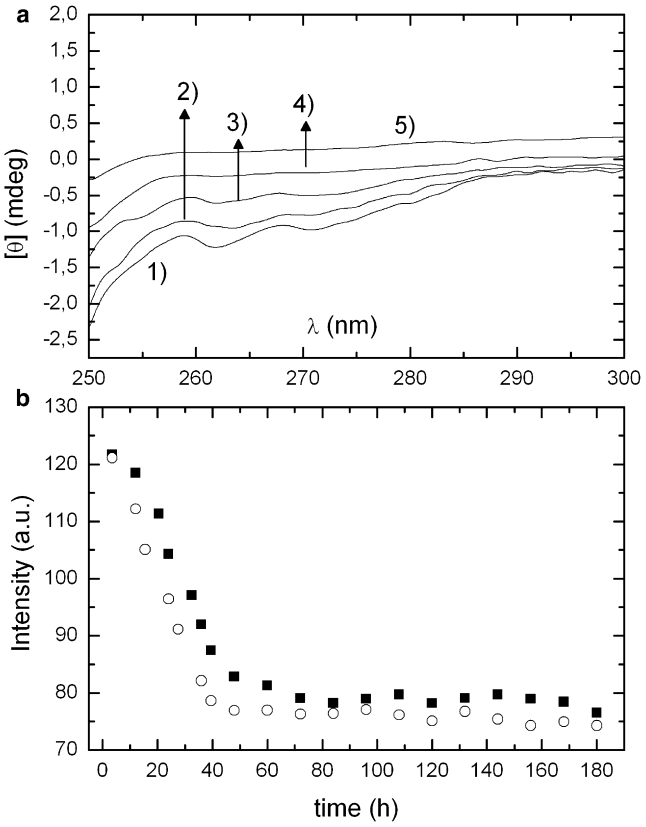

FIGURE 5 (*a*) Near-UV CD spectra of HSA solutions at pH 7.4 and 65°C in the absence of electrolyte at 1), 0 h; 2), 6 h; 3), 12 h; 4), 24 h; and 5), 48 h. (*b*) Time evolution of Trp fluorescence of HSA solutions at 65°C in the (■) absence and (○) presence of 50 mM NaCl.

In situ observation of fibrillar structures at physiological pH: TEM

TEM pictures were recorded at different stages of the incubation period for each of the conditions described above. Distinct time-dependent morphological stages can be

observed in these images. Thus, at room temperature neither fibrils nor other types of aggregates are detected, except for small amorphous protein clusters observed in the presence of electrolyte after a long incubation period (150 h), which possess a largely helical structure (Fig. 6 *a*). In contrast, when the temperature is raised to 65°C, fibril formation is observed. Electron microscopy indicates that aggregation leads first to a globular species that subsequently converts to fibrils with a curly morphology. The fibrillation pathway in the presence of electrolyte is very similar to that observed in its absence but it takes place in a shorter timescale, in agreement with previous results. Fig. 6, *b–j*, show electron micrographs of the sample heated at 65°C at different steps of the incubation period in the presence of 50 mM of electrolyte. The number and length of the fibrils has increased in relation to other structures, although several morphologies can be observed throughout incubation.

Small spherical clusters of ~20 nm formed by protein oligomers are observed (Fig. 6 *b*) at short incubation times (5 h). These aggregates present relatively few changes in their tertiary and secondary structures, as shown by CD and fluorescence data. With further incubation (Fig. 6 *c*, 15 h), a certain elongation of these spherical aggregates can be observed. This bead-like structure at short incubation times arises from what appears to be attractive interactions between spherical proteins aggregates, as shown in Fig. 6 *d-1* (see also Fig. S3), which may result in an increased exposure of hydrophobic residues, giving rise to more elongated structures. This elongation involves a conformational conversion of protein structure to consolidate the structure, and in all probability it implies changes in the hydrogen-bonding status (Fig. 6 *d-2*). This is in agreement with a further development in ThT fluorescence and decreases in both helical content and Tryp fluorescence at this incubation point, as shown previously. On the other hand, we did not find evidence of formation of elongated structures by longitudinal fusion of oligomers, as recently reported (54).

Bead-like structures progressively become more elongated upon incubation (35 h) due to mutual interactions between these structures and subsequent annealing, and convert into short protofibrils (Fig. 6 *e*), in agreement with a decrease in helical structure as revealed by CD. Alterations in the conformational structure of these oligomers and subsequent elongation via monomer addition may also be present; however, the TEM resolution did not allow us to confirm that. Several authors reported a tendency for these bead-like structures to transform into fibrillar structures at elevated temperatures caused by partial unfolding of the protein molecules and giving rise to conditions conductive to fibril formation (55–57).

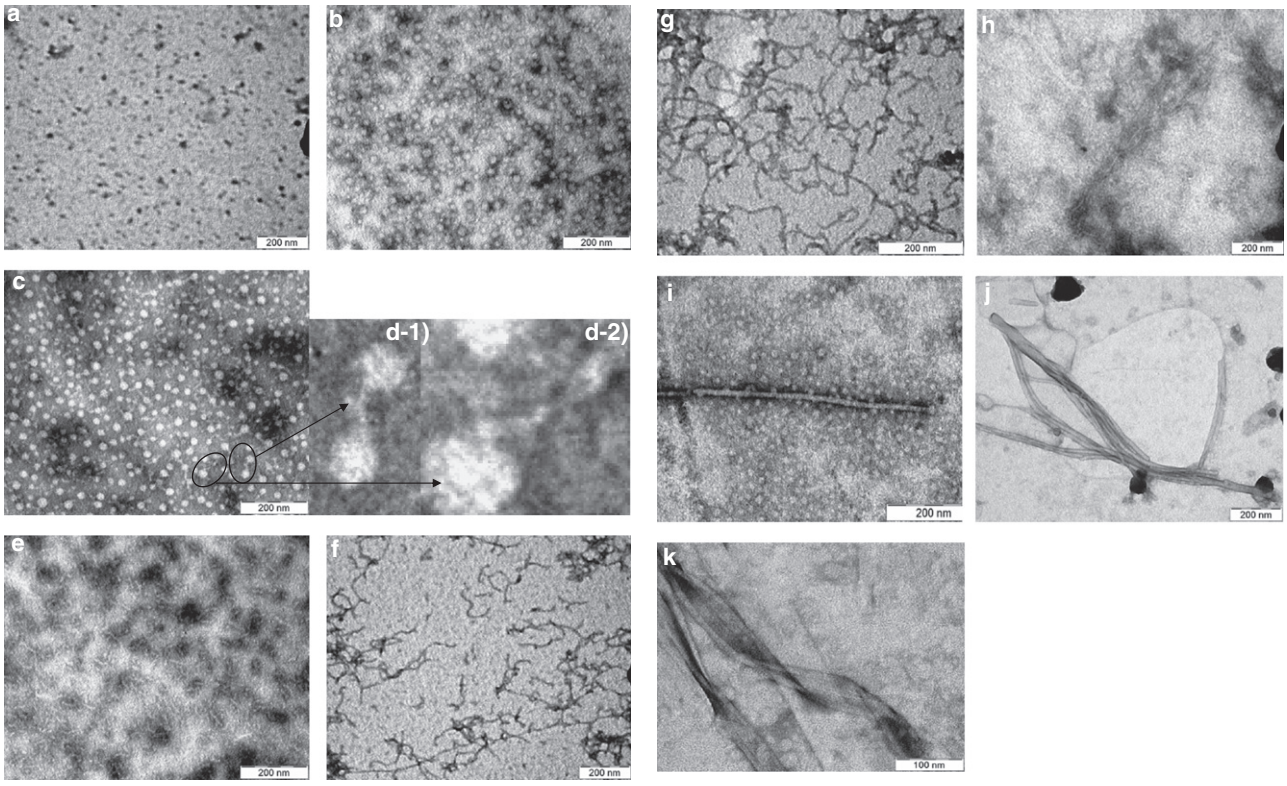

FIGURE 6 TEM pictures of the different stages of the HSA fibrillation process at pH 7.4: (*a*) at 25°C in the presence of 50 mM NaCl after 150 h of incubation, and at 65°C in the presence of 50 mM NaCl after (*b*) 5 h; (*c*) and (*d*) 15 h (part *d* shows the elongation of oligomers to give bead-like structures); (*e*) 35 h (where short protofibrils are observed); (*f*) 45 h; (*g*) 50 h (where long curly fibrils are seen); and (*h–k*) after 72 h. Part *i* shows the addition of oligomers to mature fibrils, *j* shows the association of mature fibrils in bundles, and *k* shows mature fibrils with ribbon-like structure.

Further incubation results in the presence of more fibrils, which increase in length as incubation proceeds (Fig. 6, *f* and *g*). After 2 days of incubation, numerous longer curly-branched and interconnected fibrils are present (Fig. 6 *g*), with lengths and widths characteristic of classical amyloid fibrils (i.e., between 0.5 and several micrometers in length and 9–10 nm in width (3,5,9)), as detected by TEM and AFM (see Fig. 6 *g* and Fig. S4). The appearance of this structure coincides well with the plateau region of ThT binding, the far UV-CD profiles characterized by minima around 215–220 nm, and the intermolecular β-sheet structure observed by FTIR. Most fibrils appear curly and interconnected, and some of them are even circular, as observed previously for other proteins, such as β_2 microglobulin (58) and α-crystallin (56).

If the incubation time is extended further (3 days), one can observe mature straight fibrils, which can be seen as a structural evolution of curly fibrils (Fig. 6 *h*). Mature fibrils are thicker and stiffer than single fibrils and seem to be formed by lateral (side-by-side) assembly of two or more individual filaments. These mature fibrils are less numerous in the absence of electrolyte because the electrostatic screening is lower, avoiding direct contact between constitutive fibrils. We have also observed that lateral interactions of single particles collaborate in growing these straight mature fibrils (57). Scrutiny of the protein aggregates indicates that HSA particles and clusters tend to align within the immediate vicinity of the fibers (Fig. 6 *i*), serving the single fiber as a lateral template or scaffold for small protein molecules, and would constitute a subcomponent in mature fibrils. It is worth mentioning that some fibril solutions when analyzed by SEM show the existence of very long fibers, exceeding 200 μm (see Fig. S5). We think that this effect may result from the air-drying process favoring attractive interactions between single fibers during the solvent removal.

In addition, a structural diversity of mature fibrils is noted: flat ribbons are observed in solution, as well as long, straight fibril ensembles (Fig. 6 *j*). This polymorphism may arise from variations in the quaternary structure, the manner in which protofilaments self-associate, or the protofilament substructure (e.g., in the details of hydrogen-bonding networks and side-chain packing) (59). Finally, one of the characteristic traits of the mature amyloid fibrils is their tendency to bend, twist, and agglomerate. Fig. 6 *k* shows laterally connected fibers that split over a certain distance or overlap each other. The extent and rate of this growth is dependent on solution conditions and lateral interactions between fibrils, which are responsible for the thickening of the mature fibrils and the formation of suprafibrillar aggregates. Thus, we conclude that pseudo-globular aggregates rearrange slowly to form linear, curly fibrils. These may be sufficient to produce a high-affinity template that is subsequently elongated by monomeric units or other fibrils, and can lead to the formation of ordered, straight, or ribbon-like fibrillar structures.

Fibril structure: XRD

The amyloid-like character of the fibrillar aggregates detected by TEM was confirmed by XRD. The XRD image of the HSA fibrils is shown in Fig. 7. Two strong reflections can be observed: a dominant sharp and intense reflection occurs at 4.8 Å, and one weaker, more diffuse, but still intense reflection is observed at ~11 Å. The 4.8 Å meridional reflection arises from the spacing between hydrogen-bonded individual strands in the β-sheet structure that lie perpendicular to the fibril axis, and the 11 Å equatorial reflection corresponds to the intersheet spacing, with the β-sheets stacked face to face to form the core structure of protofilaments (60,61). This indicates that fibrils possess a cross-β structure, one of the diagnostic hallmarks of amyloid structures.

Acidic conditions: kinetics and amyloid self-assembly of HSA

We next subjected HSA to acidic pH and assessed its propensity to form amyloid fibrils under such conditions in both the presence and absence of 50 mM NaCl. Increases in ThT fluorescence were observed at both 25°C and 65°C, although the increase was quite small at 25°C. This indicates the formation of a small amount of additional β-sheet conformation as a consequence of the formation of oligomeric aggregates, as will be shown below (Fig. 8). At 65°C, the increase in ThT fluorescence in the absence of electrolyte is lower than that obtained at physiological pH and extends over a larger period of time. This can be a result, on the one hand, of a lower capacity of fibrillation under these conditions (see below) or, on the other, to the presence of a lag phase if compared with solution to which electrolyte is added, as discussed further below. After a small increase in ThT fluorescence at relatively short incubation times, a plateau occurs at ~24–100 h, after which the ThT fluorescence starts to increase again. Thus, it

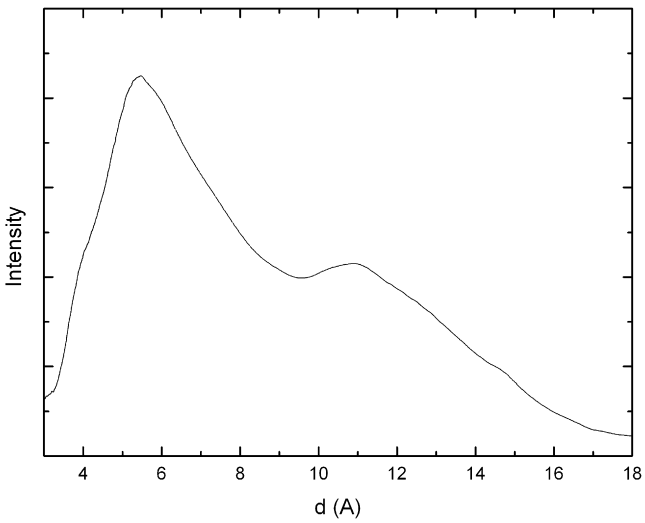

FIGURE 7 XRD pattern of HSA fibrils.

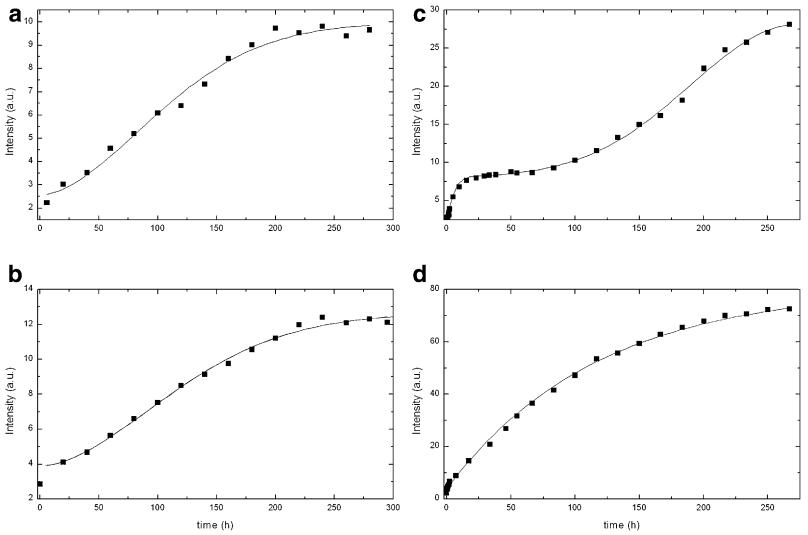

FIGURE 8 Time evolution of ThT fluorescence in HSA solutions incubated at pH 3.0 at 25°C (*a* and *b*) or 65°C (*c* and *d*) in the absence and presence of 50 mM NaCl, respectively.

is thought that under acidic conditions in the absence of electrolyte, oligomeric structures (protein clusters) are formed in a series of thermodynamically unfavorable assembly steps followed by a growth phase in which clusters are elongated by further addition of protein monomers and/or oligomers upon mutual interaction.

Fitting of the time ThT fluorescence evolution shows us that under acidic conditions, the self-assembly process becomes more cooperative, as indicated by the values of $n > 1$. This indicates the different nature of the self-assembly pathway of HSA under acidic conditions with respect to physiological pH, since interactions between protein molecules are modulated by changes in both the pH and the initial protein structure (62). In addition, the plot in the absence of electrolyte is fitted in two steps: 1), the fast formation of small clusters; and 2), the lag phase, which can originate from the necessity to reach a critical concentration of clusters for aggregation to continue. Probably, oligomeric species formed in very early stages of the aggregation process (whose existence is indicated by the slight increase of ThT fluorescence at very short incubation times) are more soluble under acidic conditions, and only after they achieve a critical concentration are they able to grow to generate larger aggregates (63). However, complete fibril formation can be achieved only in the presence of electrolyte.

Nucleation-dependent growth mechanism in acidic medium

To corroborate the origin of the plateau region in the absence of electrolyte at elevated temperature, we performed a seeding fibril growth under the conditions previously specified. When seeds are added to the protein solution, a continuous increase in ThT fluorescence is observed. This is the typical behavior observed for a nucleation-type growth mechanism and corroborates the existence of this lag phase (see Fig. S6). On the other hand, no changes are observed when protein seeds are added to a solution containing 50 mM NaCl. The difference between both solution conditions may arise from the greater hydrophobicity of oligomeric species formed during very earlier incubation stages in the presence of excess electrolyte. In its absence, electrostatic repulsion between oligomeric species seems to preclude for some time the formation of nuclei with a critical size to overcome the energy barrier that impedes aggregation.

Structural changes at acidic pH: secondary structure

At acidic pH and room temperature, both minima in $[\theta]$ at 208 and 222 nm are still present before incubation proceeds, which indicates an important retention of this type of structure, as previously described (25,64). During incubation, a slight decrease in $[\theta]$ is observed in both the absence and presence of added electrolyte, which is compatible with a small decrease in α-helices and the development of a small amount of β-sheet conformation due to the appearance of small amorphous aggregates in solution (figure not shown). In contrast, a shift of the 208 nm minimum to lower wavelengths takes place as incubation proceeds (0–200 h) at 65°C in the absence of electrolyte (Fig. 9 *a*). An increase in random coil structure (characterized by a single minimum below 200 nm) can account for this shift. Upon further incubation, an additional red shift occurs as a consequence of the increase of β-sheet structure in the aggregates formed, as also indicated by the increase in ThT fluorescence. The far-UV CD curves at 65°C in the presence of NaCl followed a trend similar to those obtained at physiological pH, although the ellipticity decrease is less severe at long incubation times as a consequence of a lower amount of scattered light from fibril aggregates (see Fig. 9 *b*). This confirms the lower fibrillar density under these conditions, which also precludes the formation of a fibrillar gel, in contrast to physiological conditions.

The secondary structure compositions in acidic solution at room temperature at the beginning of the incubation process

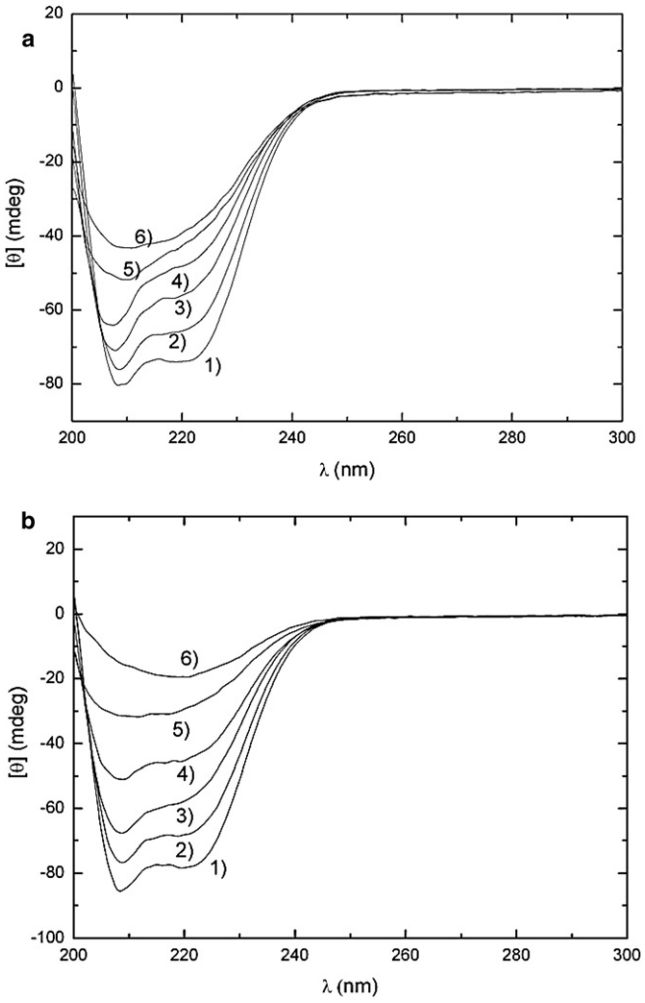

FIGURE 9 Far-UV spectra of HSA solutions at 65°C at pH 3.0 in (*a*) the absence of electrolyte at 1), 0 h; 2), 24 h; 3), 125 h; 4), 175 h; 5), 200 h; and 6), 250 h of incubation; and (*b*) the presence of 50 mM NaCl at 1), 0 h; 2), 15 h; 3), 48 h; 4), 100 h; 5), 150 h; and 6), 200 h of incubation.

indicate a reduction in α-helix conformation (~45%) and an increase in β-sheet, β-upturn, and coil contents (7%, 20%, and 28%, respectively), typical of the acid-expanded E-state of HSA (25) (Fig. 10). No significant changes were detected in structural composition during the incubation procedure at room temperature in either the absence or presence of added electrolyte up to 100 h incubation. At this stage, a slight increase in β-sheet and unordered conformations is observed for both solution conditions. In contrast, when the temperature is raised to 65°C, an important increase in β-sheets at the expense of helical conformation occurs as also observed at physiological pH. This is also accompanied by an increase in unordered conformation at early incubation times (0–150 h). The change in secondary structure occurs during a longer time interval (up to 9 days) in acidic solution. The final α-helix and β-sheet compositions are respectively 24% and 16% in the absence of electrolyte (17% and 21% in the presence of 50 mM NaCl), compared to 20% and 21% at neutral pH. This indicates small compositional changes in the resulting amyloid aggregates. The turn conformation also shows little changes throughout incubation.

FTIR experiments corroborate the structural changes undergone by the protein molecules as incubation proceeds at acidic conditions. Before incubation, the amide I band at 1650 cm^{-1} and the amide II band at 1542 cm^{-1} confirm that there is still a significant amount of α-helices. Incubation at room temperature under acidic conditions leads to a certain increase of the peak located at ~1627 nm, which corresponds to intramolecular β-sheet structure, in agreement with ThT fluorescence and CD data. On the other hand, after incubation at 65°C, a red shift of the amide I band from 1650 to 1656 cm^{-1} and a blue shift of the amide II band to 1540 cm^{-1} are indicative of an increased amount of disordered structure. In addition, the shift and further increase of the 1627 cm^{-1} peak to 1624 cm^{-1} also points to a structural transformation from an intramolecular hydrogen-bonded β-sheet to an intermolecular hydrogen-bonded β-sheet structure (46), as seen for physiological pH. Spectra also show a small high-frequency component (~1692 cm^{-1}) that would suggest the presence of antiparallel β-sheet (47) (see Fig. S7).

Structural changes at acidic pH: tertiary structure

When the pH is decreased, there is an increase in $[\theta]$ between 260 and 280 nm, and a slight decrease between 285 and 300 nm, denoting loss of tertiary structure. Nevertheless, there are still significant CD signals left, suggesting a remaining tertiary structure, in agreement with previous reports (25,65). These changes at acidic pH are related to structural rearrangements of all HSA domains. In particular, some increase in ellipticity below 295 nm takes place during incubation at room temperature, which points to little further tertiary structural changes as aggregation takes place; in particular, a loss of fine structure is detectable in the 270–295 nm region (see Fig. S8 *a*). At 65°C, changes in tertiary structure are more important; in particular, an almost complete absence of the minima is observed between 260 and 270 nm, indicating a further loss of asymmetry around disulfide bridges and/or aromatic residues as incubation proceeds. An additional loss of fine structure in the range of 280–295 nm, similar to that observed at physiological pH, is also detected (Fig. S8, *b* and *c*).

Upon incubation at acidic pH and room temperature, a certain decrease in the tryptophanyl fluorescence and a slight blue shift of the emission maximum occur between days 0 and 8 of incubation, which points to a certain internalization of Tryp to the nonpolar environment of domain II as a result of certain aggregation under these conditions (see Fig. S9). Because changes in far- and near-UV CD spectra are relatively small for this incubation period, this leads us to think that structural changes in domain II of HSA are involved in this aggregation process (66). At 65°C, the tryptophanyl residues are in a more solvent-exposed environment during the incubation because the fluorescence intensity abruptly decreases

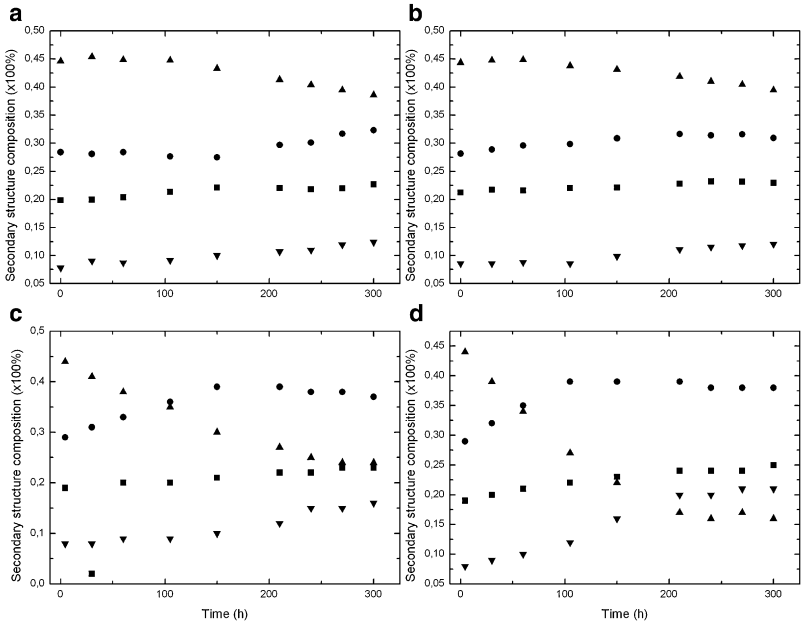

FIGURE 10 Time evolution of secondary structure compositions of HSA solutions at pH 3.0 at 25°C (*a* and *b*) or 65°C (*c* and *d*) in the absence and the presence of 50 mM NaCl, respectively. (▲) α-helix, (■) β-turn, (●) unordered, and (▼) β-sheet conformations.

during the first 4 days of incubation as a result of the sequential unfolding of domains I and II of HSA. This period of time is slightly shorter than at pH 7.4 (mainly in the presence of electrolyte excess) because the expanded E state already involves an important alteration in the tertiary structure.

In situ observation of fibrillar structures at acidic pH: TEM

HSA samples obtained at different incubation times were also subjected to TEM analysis under acidic conditions. At room temperature in the absence of salt, no aggregates were observed during the first 2 days of the incubation process. From the third day, the presence of small clusters (globules) of aggregated protein could be observed. These aggregates have a globular or spherical shape, not the regular fibrillar appearance associated with amyloid structures (see Fig. 11 *a*). In addition, less numerous, more elongated aggregates (20–30 nm long, 3–4 nm wide) can be also observed, and their population slightly increases as incubation proceeds. The formation of these types of aggregates is characterized by a decrease of helical structure accompanied by a slight rise in β-sheet and unordered conformations from CD measurements at long incubation times.

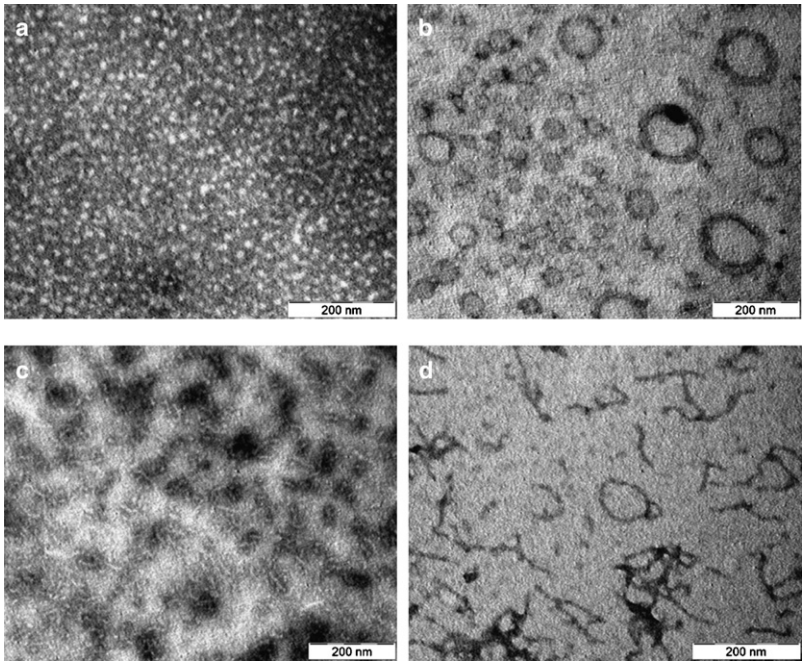

FIGURE 11 TEM pictures of the different stages of the HSA fibrillation process at pH 3.0 in the presence of 50 mM NaCl (*a*) at 25°C after 150 h of incubation, and at 65°C after (*b*) 24 h, (*c*) 150 h, and (*d*) 250 h of incubation in the presence of 50 mM NaCl.

When the temperature is raised to 65°C, fibril formation takes place in several steps. First, formation of quasi-spherical aggregates takes place under incubation times similar to those at pH 7.4, and these seem to be fairly soluble. On the other hand, we have found that a coexistence of spherical aggregates with circular ring-shaped particles of larger size (~100–300 nm) is observed at short incubation times (on the order of a few hours) in the presence of excess electrolyte (Fig. 11 *b*). These structures appear as a possible intermediate structural rearrangement of smaller protein aggregates before fibril formation facilitated by electrostatic screening. There is no evidence as to whether structural reorganization to form fibrils takes place within this type of aggregates, or whether dissociation of HSA molecules from these structures occurs. Based on our CD data, which indicate that a progressive gaining of β-sheet structure and unordered conformation at the expense of α-helices takes place in the first part of the incubation process, we suggest that only after a certain critical amount of β-sheet structure is reached inside these ring-shaped particles will short fibrils be formed in solution from decomposition of the former and become stable. Once sufficient molecules are present within the oligomer, reorganization steps become thermodynamically favorable as a result of an increase in the number of hydrogen bonds and other stabilizing interactions. Once fragments of highly ordered aggregates are present, the free energy for addition of monomeric molecules to a growing fibril will become more favorable. Similar circular ring-shaped structures have also been observed as a structural intermediate before the formation of amyloid fibrils in the self-assembly process of insulin (67), A$\beta_{17\text{-}42}$ peptide (68), A$\beta_{1\text{-}4}$ peptide, and HaPrP23-144 prion protein (69). In this case, the circular structures may incorporate into fibrils but also self-aggregate to form large, amorphous structures (57). Given the large structural differences between HSA insulin and A$\beta_{17\text{-}42}$ peptide, and their distinct propensity to form amyloid fibrils, it seems reasonable to think that these circular ring-shaped structures can be a sort of common structural intermediate of amyloid fibril formation under different solution conditions.

After longer incubation times (6 days) for HSA solutions in the absence of electrolyte at 65°C, small, well-defined, short protofibrils (~100 nm long and 3–4 nm wide) start to appear (Fig. 11 *c*). The corresponding CD spectrum shows a progressive increase in the proportion of β-structure at the expense of the helical one during incubation. In contrast, the presence of electrolyte involves an additional step: the formation of short curly fibers occurs in a broader incubation timescale than at physiological pH (Fig. 11 *d*); under further incubation, the fibrils appear to increase slightly in number and length. They range from ~100 nm to several hundred nanometers in length and 8 to 11 nm in width; thus, they are shorter on average than those obtained at physiological conditions but have the same average width. Closed fibril loops with diameters of ~100 nm were also frequently observed because the formed filaments can remain short and thin to enable them to bend and form closed rings, as also observed for β_2 microglobulin (58), α-crystallin (56), equine lysozyme (70), insulin (67), and α-synuclein (71). This fibrillar material appears similar to protofilaments observed in the early stages of other amyloidogenic systems, given the small length and the absence of higher-order structures.

DISCUSSION

The ability to form amyloid fibrils is a generic property of polypeptide chains, although the propensity of different regions of proteins to form such structures varies substantially (72). The properties of unfolded polypeptides, including their relative propensities for α- and β-structure, their intrinsic solubility, and the nature of the interactions within the resultant fibrillar structures, are likely to be particularly important determinants in their relative abilities to form fibrils. The conformation of the partially folded state is not by itself a critical feature of fibril formation; rather, it is suggested that the basis for amyloidogenesis is the presence of partially denaturation conditions that destabilize the native fold of the protein but do not preclude noncovalent interactions between the various groups within the protein. In our case, it appears necessary to destabilize HSA molecules and hence to generate a partially folded intermediate that can aggregate to form fibrils. Thus, one can readily atttain conditions in which such aggregation-prone intermediate states are significantly populated by lowering the pH or raising the temperature. ThT fluorescence, CR staining, XRD, and TEM pictures demonstrate the formation of amyloid-like structures under these conditions. The aggregation process is governed by the balance between attractive and repulsive interactions between protein molecules. Conformational changes induced by heat increase the number of hydrophobic residues exposed to the aqueous solvent. The exposure of these groups results in attractive hydrophobic interactions that play a dominant role in the aggregation process. Repulsive forces are induced by a surface charge that can be modulated by changes in pH, which controls the net charge of the protein, and by the ionic strength of the solvent, which controls the screening of electrostatic interactions (73).

Absence of a lag phase in HSA fibrillation process in most solution conditions

A first characteristic of the HSA fibrillation process is the absence of a lag phase, as previously observed for bovine serum albumin (BSA) (74) and acyl phosphatase (75) under all solutions conditions analyzed except for acidic pH at room temperature. This occurs if the initial aggregation is a downhill process that does not require a highly organized and unstable nucleus. This is supported by the fact that seeding of preformed aggregates does not accelerate the fibrillation process. In this regard, it has been suggested that large multidomain proteins like BSA are able to form

propagation-competent nucleus-like structures (oligomeric structures) (74). In our case, TEM pictures also show the formation of spherical oligomers upon very short incubation times, which occur by a means of classical coagulation mechanism. In contrast, the presence of a certain lag phase upon incubation in acidic medium at 65°C in the absence of electrolyte may well indicate that oligomeric aggregates need more time to develop and/or persist for longer times because of their enhanced solubility, so they need to reach a certain number or size to change the energy landscape of the system and promote further aggregation.

Existence of different intermediates on the HSA fibrillation pathway

On a macroscopic scale, the different steps in the fibril formation pattern, as observed by TEM, consist of the formation of nonfibrillar aggregates (oligomeric globules) and their subsequent elongation (bead-like structures and circular ring-shaped structures), and the development of protofilaments and their assembly in fibrils, which can rearrange in more complex structures. On a molecular level, CD and FTIR results show that HSA possesses native-like α-helical characteristics with residual β-sheet content before acidic or heat treatment.

In very early periods of incubation, HSA forms small, soluble, globular oligomers of mainly native-like molecules in acidic, physiological, and/or high-temperature conditions, with a progressive increase in β-sheet content and unordered conformation upon further incubation, as revealed by ThT fluorescence and far-UV CD. Thus, upon further incubation (5–50 h) at elevated temperature, the spectroscopic characteristics indicate losses of persistent tertiary structure along with unfolding of certain secondary structure to different extents depending on the solution conditions (acidic or physiological pH, added salt). Different conditions may cause different regions of the polypeptide chains that are relatively flexible and not involved in strong intramolecular interactions (76,77) to enhance the aggregation process, leading to an evolution of the previous globules into additional intermediate structures (bead-like structures and circular ring-shaped structures at physiological and acidic pH, respectively, with the latter found only at high ionic strength). Bead-like structures arise from what appears to be attractive interactions between globular protein oligomeric clusters, which may result from an increased exposure of hydrophobic residues, mainly in the presence of electrolyte. We found no evidence of formation of elongated structures by longitudinal fusion of oligomers. These bead-like structures progressively become more elongated upon incubation (35 h) due to mutual interactions between them and convert into protofibrils, in agreement with a decrease in helical structure as indicated by CD data. The decrease in diameter accompanying elongation may be explained on the basis of reorganization of structure, in particular of the β-strands. Several authors have also reported the tendency of these bead-like structures to transform into fibrillar structures at elevated temperatures caused by partial unfolding of the protein molecules and giving rise to conditions conducive to fibril formation (55–57), as shown in Fig. 6 *d*.

The combination of experimental observations described here indicates that the formation of fibrils from soluble HSA molecules proceeds in a series of stages, the first of which is effectively the presence of oligomeric globules. Thus, the role of association-competent oligomeric intermediates may result in a kinetic pathway via clustering of these oligomeric species, which can be rationalized in the light of colloid coagulation theory, i.e., the formation of a critical oligomer or an ensemble of critical oligomers and subsequent aggregation into bead-like structures, and then protofibrillar structures (78). The persistence of these spherical oligomers in solution coinciding with fibril assembly also supports the view that they may be ''on-pathway'' intermediates (see Fig. 6 and Fig. S10). Spherical oligomeric structures have been proposed to serve a key, on-pathway role in both the formation and elongation of amyloid fibrils of the Sup35 (79) and Ure2p yeast prion proteins (80).

In contrast, we speculate that the circular ring-shaped structures found in acidic medium at high ionic strength, which appear to be composed of two semicircular units, may come from bending and association of early-formed, short, bead-like structures due to a decrease in their solubility. This decrease would stem from the electrolyte concentration present in solution, which screens electrostatic interactions between aggregates. Once sufficient molecules are present within this type of intermediate structure, reorganization steps become thermodynamically favorable as a result of an increase in the number of hydrogen bonds and other stabilizing interactions. Once critical fragments of ordered aggregates are present (with a critical amount of β-sheet structure), the free energy for addition of monomeric molecules to a growing elongated structure becomes more favorable. In this way, short protofibrils will be formed in solution upon dissolution of the ring-shaped intermediate structures and will become stable. These intermediates are not observed by TEM once protofibrils start to be observed, which suggests that they may act as reservoirs of the initially very short protofibrils. However, a deeper structural analysis of this structural intermediate and its evolution to protofibrils is needed, and is currently under way. On the other hand, the fact that some elongated structures (but not fibrils) are formed in acidic pH at room temperature, in contrast to physiological medium, for which no aggregation is observed except for some amorphous aggregates, suggests that the charge distribution on the protein influences the propensity to form amyloid fibrils. The neutralization of negative charges at acidic pH may promote this elongation.

HSA fibrils are curly

The thermodynamic instability of prefibrillar aggregates causes them to evolve into more stable assemblies upon additional incubation (>75 h), eventually leading to the appearance

of stable fibrils, mainly at physiological conditions at elevated temperatures, where structural reorganization results in the large majority of hydrophobic groups being concealed from the solvent. This is corroborated by ThT fluorescence, far UV-CD, and FTIR spectra, which demonstrate that the major elements of ordered secondary structure are β-sheets, suggesting that the α-helical regions of the native protein have undergone significant structural changes. TEM pictures corroborate this picture, showing that the fibrils formed are mainly, narrow, branched, and elongated but curly, in contrast to the straight needle-like structures characteristic of bona fide fibrils. As incubation proceeds, these worm-like structures increase in length. These fibrils display the typical 4.8 Å peak indicating the typical interstrand distance of classical fibrils, and the 11 Å equatorial reflection corresponds to the intersheet spacing, with the β-sheets stacked face to face to form the core structure of protofilaments (81). Based on the CD and FTIR data, we speculate that these types of fibrils may be formed by a seam of β-sheet structure decorated by relatively disorganized α-helical structure, as previously observed for RNase A (82) or yeast Ure2p (83). In addition, an antiparallel arrangement of β-strands forming the β-sheet structure of the HSA fibrils seems to be the most probable configuration, as denoted by the band at ~1691–1693 cm^{-1} in the FTIR spectra. Curly aggregates have been also seen in other proteins, such as β_2 microglobulin (58) and α-crystallin (56). In addition, intramolecular end-to-end association of short individual filaments appears to be favorable, as TEM images reveal the presence of a substantial number of closed loops appearing to form spontaneously, mainly in the absence of electrolyte at acidic conditions. Qualitatively, the probability of a single fibril joining end-to-end to form a closed loop will be high if the fibril is sufficiently flexible and of appropriate length for the ends to find themselves regularly in close proximity to each other (84). Indeed, the results presented here exemplify the favorable nature of loop formation when such fibril morphologies are adopted. Loop formation was reported previously for other amyloid-forming systems (85,86).

On the other hand, it is interesting to note that a similar curly morphology for HSA can be achieved under different solution conditions: the single filament, in the form of both open flexible chains and closed loops, is observed at both physiological and acidic pH in the presence of electrolyte. Nevertheless, the rate and extent of aggregation depends on the solution conditions: the amount of formed fibrils and their length (larger at physiological conditions) favor interactions between early aggregates to form fibrils. This is revealed by the formation of a gel phase under suitable solution conditions.

Curly fibers can evolve into a suprafibrillar structure

Very long incubation times (>150 h) lead to a more complex morphological variability among amyloid fibrils (e.g., long straight fibrils, flat-ribbon structures, or laterally connected fibers). These compact, mature fibrillar assemblies formed at the endpoint of the aggregation process may result from an effort to minimize the exposure of hydrophobic residues, and are also likely to result in increased van der Waals interactions, leading to greater stability, as previously noted for β_2-microglobulin (87), α-synuclein (5), and insulin (88). A similar progression in structure from curly fibrils to mature straight fibers was also observed for Aβ-peptide (89) and insulin (90). In contrast, BSA fibrillation was shown to be halted at the early curly stage, despite the enormous structural similarities with HSA, since no further development in fibrillar structure over long timescales was observed (74). Mature fibrils are thicker and stiffer than single fibrils and appear to be formed by lateral (side-by-side) assembly of two or more individual filaments. Nevertheless, under physiological conditions, we observed that mature straight fibrils can also grow by swollen protein particles tending to align within the immediate vicinity of the fibers, as shown in Fig. 6 *i*, serving the single fiber as a lateral template or scaffold for small protein molecules, and would constitute a subcomponent in mature fibrils. Their population is dependent on solution conditions and lateral interactions between fibrils. This may be an additional pathway to the formation of mature fibrils via association of protofibrils. Conformational preferences for a certain pathway to become active may exist, and thus the influence of environmental conditions such as pH, temperature, and salt must be considered. Thus, it seems that a single filament may act as a ''lateral template'' or scaffold for small protein particles, which would constitute a neighboring subcord-like feature in the fiber shown in Fig. 6 *h*. This filament + monomers/oligomers scenario is an alternative pathway to the otherwise dominating filament + filament manner of the protein fibril's lateral growth, as has been also observed for insulin (57). AFM data recently reported by Green et al. (91) suggest that mature fibrils from human amylin are unlikely to be assembled by the lateral association of protofibrils.

It appears, therefore, that even for a homogeneous HSA sample undergoing uniform temperature or acidic treatment, there is still more than one mode of assembly of filaments (92). Such polymorphism may be caused by differences in the number of filaments assembled in the mature fibrils; however, it may also result from the incorporation in different regions of the sequence of the polypeptide chain with various types of fibrils. In addition, the differences between the populations of fibers clearly involve not only the rate of the aggregation process, but also the different quaternary folds. Although the different distribution profiles of the fibrillar features may still be explained in terms of kinetic effects (e.g., temperature may differently affect the kinetics at various stages of the assembly, effectively marginalizing certain sequential processes), high temperatures may also have a more direct effect on amyloidogenesis, for instance, by increasing the thermal energy of the interacting molecules

and hence causing the alignment of filaments to become less accurate. Such unspecific effects may contribute to morphological differences in any protein's amyloid samples induced at high temperature. In this regard, recent reports based on nuclear magnetic resonance showed that different fibril morphologies have different underlying secondary structures, and as such are likely produced by distinct independent assembly pathways (93,94).

A summary of the various fibril morphologies observed in this study is shown in Fig. 12 together with a schematic representation of the assembly process. We propose that at elevated temperature (except at pH 3.0 in the absence of electrolyte), HSA forms rapidly globular oligomers that upon mutual interaction evolve into more elongated structures (bead-like) that grow to protofibrils either by subsequent annealing of oligomers and/or protein monomers. Mature fibrils can be formed by lateral association of protofibrils or the addition of protein oligomers to the growing fibril, both at the ends of the fibril and by lateral fusion. Ring-like structures are present in acidic conditions at elevated temperature in the presence of electrolyte as an additional intermediate state formed by association of short bead-like structures, which disappears when protofibrils are observed in solution. Thus, we think that they may act as reservoirs of initially very short protofibrils.

CONCLUSIONS

We observed the formation of protofibrils, curly fibers, and mature fibrils by the protein HSA under different solution conditions. We analyzed the fibrillation process and the conformational changes associated with it by using different spectroscopic techniques, and confirmed the necessary development of β-sheet structure upon fibrillation. In addition, the shapes of the different structural intermediates and final products in the fibrillation process were observed by TEM, SEM, and AFM. The obtained fibrils show structural features typical of classical amyloid fibers, as denoted by XRD, CD, and fluorescence spectroscopies, and TEM. A model of fibril formation based on the elongation of protein oligomers through mutual interactions and subsequent annealing and growth is presented. Nevertheless, some differences in the fibrillation mechanism occur depending on the solution conditions; for example, ring-shaped structures are observed only as a structural intermediate under acidic conditions in the presence of added electrolyte.

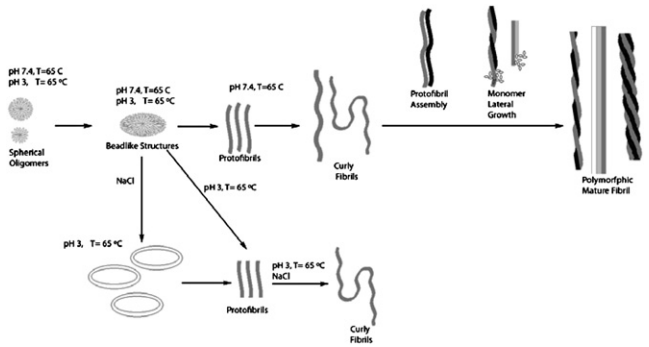

FIGURE 12 Mechanisms of fibril formation for HSA.

SUPPORTING MATERIAL

Ten figures and a table are available at http://www.biophysj.org/biophysj/supplemental/S0006-3495(09)00322-1.

We thank Dr. Eugenio Vázquez for his assistance with the CD measurements.

This study was supported by the Ministerio de Educación y Ciencia (project MAT-2007-61604).

REFERENCES

1. Reches, M., and E. Gazit. 2003. Casting metal nanowires within discrete self-assembled peptide nanotubes. *Science.* 300:625–627.
2. Rajagopal, K., and J. P. Schneider. 2004. Self-assembling peptides and proteins for nanotechnological applications. *Curr. Opin. Struct. Biol.* 14:480–486.
3. Stefani, M., and C. M. Dobson. 2003. Protein aggregation and aggregate toxicity: new insights into protein folding, misfolding diseases and biological evolution. *J. Mol. Med.* 81:678–699.
4. Soto, C., L. Estrada, and J. Castilla. 2006. Amyloids, prions and the inherent infectious nature of misfolded protein aggregates. *Trends Biochem. Sci.* 31:150–155.
5. Khurana, R., C. Ionescu-Zanetti, M. Pope, J. Li, L. Nelson, et al. 2003. A general mode for amyloid fibril assembly based on morphological studies using atomic force microscopy. *Biophys. J.* 85:1135–1144.
6. Chiti, F., M. Stefani, N. Taddei, G. Ramponi, and C. M. Dobson. 2003. Rationalization of the effects of mutations on peptide and protein aggregation rates. *Nature.* 424:805–808.
7. Williams, A. D., E. Portelius, I. Kheterpal, J. T. Guo, K. D. Cook, et al. 2004. Mapping a β amyloid fibril secondary structure using scanning proline mutagenesis. *J. Mol. Biol.* 335:833–842.
8. Hortscansky, P., T. Christopeit, V. Schroeckh, and M. Fändrich. 2005. Thermodynamic analysis of the aggregation propensity of oxidized Alzheimer's β-amyloid variants. *Protein Sci.* 14:2915–2918.
9. Fändrich, M., V. Forge, K. Buder, M. Kittler, C. M. Dobson, et al. 2003. Myoglobin forms amyloid fibrils by association of unfolded peptide segments. *Proc. Natl. Acad. Sci. USA.* 100:15463–15468.
10. Gazit, E. 2002. The ''correctly folded'' state of proteins: is it a metastable state? *Angew. Chem. Int. Ed. Engl.* 41:257–259.
11. Gillmore, J. D., A. J. Stangou, G. A. Tennet, D. R. Booth, J. O'Grady, et al. 2001. Clinical and biochemical outcome of hepatorenal transplantation for hereditary systemic amyloidosis associated with apolipoprotein AI Gly26Arg. *Transplantation.* 71:986–992.
12. Carulla, N., G. L. Caddy, D. R. May, J. Zurdo, M. Gairi, et al. 2005. Molecular recycling within amyloid fibrils. *Nature.* 436:554–558.
13. Pepys, M. B., J. Herbert, W. L. Hutchison, G. A. Tennent, H. J. Lachmann, et al. 2002. Targeted pharmacological depletion of serum amyloid P component for treatment of human amyloidosis. *Nature.* 417:254–259.
14. Janus, C., M. A. Chishti, and D. Westaway. 2000. Transgenic mouse models of Alzheimer's disease. *Biochim. Biophys. Acta.* 1502:63–75.
15. Cohen, F. E., and J. W. Kelly. 2003. Therapeutic approaches to protein-misfolding diseases. *Nature.* 426:905–909.
16. Tanaka, M., P. Chien, N. Narber, R. Cooke, and J. S. Weissman. 2004. Conformational variations in an infectious protein determine prion strain differences. *Nature.* 428:323–328.

17. Fändrich, M., and C. M. Dobson. 2002. The behavior of polyamino acids reveals an inverse side chain effect in amyloid structure formation. *EMBO J.* 21:5682–5690.
18. Gorinstein, S., A. Caspi, A. Rosen, I. Goshev, M. Zemser, et al. 2002. Structure characterization of human serum aproteins in solution and dry state. *J. Pept. Res.* 59:71–78.
19. Taboada, P., S. Barbosa, E. Castro, and V. Mosquera. 2006. Amyloid fibril formation and other aggregate species formed by human serum albumin association. *J. Phys. Chem. B.* 110:20733–20736.
20. Pace, C. N., F. Vajdos, L. Fee, G. Grimsley, and T. Gray. 1995. How to measure and predict the molar absorption coefficient of a protein. *Protein Sci.* 4:2411–2423.
21. Sreerama, N., and R. W. Woody. 2000. Estimation of protein secondary structure from circular dichroism spectra: comparison of CONTIN, SELCON, and CDSSTR methods with an expanded reference set. *Anal. Biochem.* 287:252–260.
22. Uversky, V. N., and A. L. Fink. 2004. Conformational constraints for amyloid fibrillation: the importance of being unfolded. *Biochim. Biophys. Acta.* 1698:131–153.
23. Calamai, M., F. Chiti, and C. M. Dobson. 2005. Amyloid fibril formation can proceed from different conformations of a partially unfolded protein. *Biophys. J.* 89:4201–4210.
24. Morel, B., S. Casares, and F. A. Conejo-Lara. 2006. Single mutation induces amyloid aggregation in the α-spectrin SH3 domain: analysis of the early stages of fibril formation. *J. Mol. Biol.* 356:453–468.
25. Dockal, M., D. C. Carter, and F. Rüker. 2000. Conformational transitions of the three recombinant domains of human serum albumin depending on pH. *J. Biol. Chem.* 275:3042–3050.
26. Peters, T. Jr., 1996. All About Albumin: Biochemistry, Genetics and Medical Application. Academic Press, New York.
27. Geisow, M. J., and G. H. Beaven. 1977. Physical and binding properties of large fragments of human serum albumin. *Biochem. J.* 165:477–484.
28. Khan, M. Y. 1986. Direct evidence for the involvement of domain III in the N-F transition of bovine serum albumin. *Biochem. J.* 236:307–310.
29. Ahmad, B., M. K. A. Khan, S. Haq, and R. H. Khan. 2004. Intermediate formation at lower urea concentration in 'B' isomer of human serum albumin: a case study using domain specific ligands. *Biochem. Biophys. Res. Commun.* 314:166–173.
30. Taboada, P., S. Barbosa, E. Castro, M. Gutiérrez-Pichel, and V. Mosquera. 2007. Effect of solvation on the structure conformation of human serum albumin in aqueous-alcohol mixed solvents. *Chem. Phys.* 340:59–68.
31. Farruggia, B., F. Rodriguez, R. Rigatuso, G. Fidelio, and G. Picó. 2001. The participation of human serum albumin domains in chemical and thermal unfolding. *J. Protein Chem.* 20:81–89.
32. Flora, K., J. D. Brennan, G. A. Baker, M. A. Doody, and F. V. Bright. 1998. Unfolding of acrylodan-labeled human serum albumin probed by steady-state and time resolved fluorescence methods. *Biophys. J.* 75:1084–1096.
33. Rader, A. J., B. M. Hespenheide, K. A. Kuhn, and M. F. Thorpe. 2002. Protein unfolding: rigidity lost. *Proc. Natl. Acad. Sci. USA.* 99: 3540–3545.
34. LeVine, H. 3rd., 1993. Thioflavine T interaction with synthetic Alzheimer's disease β-amyloid peptides: detection of amyloid aggregation in solution. *Protein Sci.* 2:404–410.
35. Klunk, W. E., J. W. Pettegrew, and D. J. Abraham. 1989. Quantitative evaluation of Congo Red binding to amyloid-like proteins with a β-pleated sheet conformation. *J. Histochem. Cytochem.* 37:1273–1281.
36. Khurana, R., C. Coleman, C. Ionescu-Zanetti, S. A. Carter, V. Krishna, et al. 2005. Mechanisms of thioflavin T binding to amyloid fibrils. *J. Struct. Biol.* 151:229–238.
37. Sagis, L. M. C., C. Veerman, and E. Van der Linden. 2004. Mesoscopic properties of semiflexible amyloid fibrils. *Langmuir.* 20:924–927.
38. Morozova-Roche, L. A., J. A. Jones, W. Noppe, and C. M. Dobson. 1999. Independent nucleation and heterogeneous assembly of structure during unfolding of equine lysozime. *J. Mol. Biol.* 289:1055–1073.
39. Jund, P., R. Jullien, and I. Campbell. 2001. Random walks on fractals and stretched exponential relaxation. *Phys. Rev. E.* 63:361311–361314.
40. Harper, J. D., and P. T. J. Landsbury. 1997. Models of amyloid seeding in Alzheimer's disease and scrapie: mechanistic truths and physiological consequences of the time-dependent solubility of amyloid proteins. *Annu. Rev. Biochem.* 66:385–407.
41. Lomakin, A., D. S. Chung, G. B. Benedek, D. A. Kirschner, and D. B. Teplow. 1996. On the nucleation and growth of amyloid β-protein fibrils: detection of nuclei and quantitation of rate constants. *Proc. Natl. Acad. Sci. USA.* 93:1125–1129.
42. Lomakin, A., D. B. Teplow, D. A. Kirschner, and G. B. Benedek. 1997. Kinetic theory of fibrillogenesis of amyloid β-protein. *Proc. Natl. Acad. Sci. USA.* 94:7942–7947.
43. Ferrone, F. 1999. Analysis of protein aggregation kinetics. *Methods Enzymol.* 309:256–274.
44. Susi, H., and D. M. Byler. 1983. Protein structure by Fourier transform infrared spectroscopy: second derivative spectra. *Biochem. Biophys. Res. Commun.* 115:391–397.
45. Lin, S. -Y., Y. -S. Wei, M. -J. Li, and S. -L. Wang. 2004. Effect of ethanol or/and captopril on the secondary structure of human serum albumin before and after protein binding. *Eur. J. Pharm. Biopharm.* 57:457–464.
46. Jackson, M., and H. H. Mantsch. 1995. The use and misuse of FTIR spectroscopy in the determination of protein structure. *Crit. Rev. Biochem. Mol. Biol.* 30:95–120.
47. Casal, H. L., U. Kohler, and H. H. Mantsch. 1988. Structural and conformational changes of β-lactoglobulin B: an infrared spectroscopy study of the effect of pH and temperature. *Biochim. Biophys. Acta.* 957:11–20.
48. Fabian, H., L. -P. Choo, G. I. Szendrei, M. Jackson, W. C. Halliday, et al. 1993. Infrared spectroscopic characterization of Alzheimer plaques. *Appl. Spectrosc.* 47:1513–1518.
49. Lin, S. -Y., Y. -S. Wei, M. -J. Li, and S. -L. Wang. 2004. Effect of ethanol or/and captopril on the secondary structure of human serum albumin before and after protein binding. *Spectrochim. Acta [A].* 60:3107–3111.
50. Uversky, V. N., N. V. Narizhneva, T. V. Ivanova, and A. Y. Tomashevski. 1997. Rigidity of human α-fetoprotein tertiary structure is under ligand control. *Biochemistry.* 494:13638–13645.
51. Muzammil, S., Y. Kumar, and S. Tayyab. 1999. Molten globule-like state of human serum albumin at low pH. *FEBS Lett.* 266:26–32.
52. Qiu, W., L. Zhang, O. Okobiah, Y. Yang, L. Wang, et al. 2006. Ultrafast solvation dynamics of human serum albumin: correlations with conformational transitions and site-selected recognition. *J. Phys. Chem. B.* 110:10540–10549.
53. Cowgill, R. W. 1968. Fluorescence and protein structure. XIV. Tyrosine fluorescence in helical muscle proteins. *Biochim. Biophys. Acta.* 161:431–438.
54. Shahi, P., R. Sharma, S. Sanger, I. Kumar, and R. S. Jolly. 2007. Formation of amyloid fibrils via longitudinal growth of oligomers. *Biochemistry.* 46:7365–7373.
55. Burgio, M. R., P. M. Bwennet, and J. F. Koretz. 2001. Heat-induced quaternary transitions in hetero- and homo-polymers of α-crystallin. *Mol. Vis.* 7:228–233.
56. Meehan, S., Y. Berry, B. Luisa, C. M. Dobson, J. A. Carver, et al. 2004. Amyloid fibril formation by lens crystallin proteins and its implications for cataract formation. *J. Biol. Chem.* 279:3413–3419.
57. Jansen, R., W. Dzwolak, and R. Winter. 2005. Amyloidogenic self-assembly of insulin aggregates probed by high resolution atomic force microscopy. *Biophys. J.* 88:1344–1353.
58. Radford, S. E., W. S. Gosal, and G. W. Platt. 2005. Towards an understanding of the structural molecular mechanism of β2-microglobulin amyloid formation *in vitro*. *Biochim. Biophys. Acta.* 1753:51–63.
59. Kodali, R., and R. Wetzel. 2007. Polymosphism in the intermediates and products of amyloid assembly. *Curr. Opin. Struct. Biol.* 17:48–57.
60. Sunde, M., and C. Blake. 1997. The structure of amyloid fibrils by electron microscopy and X-ray diffraction. *Adv. Protein Chem.* 50:123–159.

61. Bouchard, M., J. Zurdo, E. J. Nettleton, C. M. Dobson, and C. V. Robinson. 2000. Formation of insulin amyloid fibrils followed by FTIR simultaneously with CD and electron microscopy. *Protein Sci.* 9:1960–1967.

62. Vetri, V., F. Librizzi, M. Leone, and V. Militello. 2007. Thermal aggregation of bovine serum albumin at different pH: comparison with human serum albumin. *Eur. Biophys. J.* 36:717–725.

63. Bader, R., R. Bamford, J. Zurdo, B. F. Luisi, and C. M. Dobson. 2006. Probing the mechanism of amyloidogenesis through a tandem repeat of the PI3–SH3 domain suggests a generis model for protein aggregation and fibril formation. *J. Mol. Biol.* 356:189–208.

64. Shaw, A. K., and S. K. Pal. 2008. Spectroscopic studies on the effect of temperature on pH-induced folded states of human serum albumin. *J. Photochem. Photobiol. B.* 90:69–77.

65. Ahmad, B., S. Parveen, and R. H. Khan. 2006. Effect of albumin conformation on the binding of ciprofloxacin to human serum albumin: a novel approach directly assigning binding site. *Biomacromolecules.* 7:1350–1356.

66. Eftink, M. R., and C. A. Ghiron. 1976. Exposure of tryptophyl residues in proteins. Quantitative determination by fluorescence quenching studies. *Biochemistry.* 15:672–679.

67. Sibley, S. P., K. Sosinsky, L. E. Gulian, E. J. Gibbs, and R. F. Pasternack. 2008. Probing the mechanism of insulin aggregation with added metalloporphyrins. *Biochemistry.* 47:2858–2865.

68. Zheng, J., H. Jang, B. Ma, and R. Nussinov. 2008. Annular structures as intermediates in fibril formation of Alzheimer Aβ_{17-42}. *J. Phys. Chem. B.* 112:6856–6865.

69. Moore, R. E., S. F. Hayes, E. R. Fischer, and S. A. Priola. 2007. Amyloid formation via supramolecular peptide assemblies. *Biochemistry.* 46:7079–7087.

70. Malisauskas, M., V. Zamotin, J. Jass, W. Noppe, C. M. Dobson, et al. 2003. Amyloid protofilaments from the calcium-binding protein equine lysozyme: formation of ring and linear structures depends on pH and metal ion concentration. *J. Mol. Biol.* 330:879–890.

71. Lashuel, H. A., D. Hartley, B. M. Petre, T. Walz, and P. T. Lansbury Jr. 2002. Neurodegenerative disease: amyloid pores from pathogenic mutations. *Nature.* 418:291.

72. Jarrett, J. T., and P. T. Lansbury Jr. 1992. Amyloid fibril formation requires a chemically discriminating nucleation event—studies of an amyloidogenic sequence from the bacterial protein OSMB. *Biochemistry.* 31:12345–12352.

73. Lefebvre, J., D. Renard, and A. C. Sánchez-Gimeno. 1998. Structure and rheology of heat-set gels of globular proteins. I. Bovine serum albumin gels in isoelastic conditions. *Rheol. Acta.* 37:345–357.

74. Holm, N. K., S. K. Jespersen, L. V. Thomassen, T. Y. Wolff, P. Sehgal, et al. 2007. Aggregation and fibrillation of bovine serum albumin. *Biochim. Biophys. Acta.* 1774:1128–1138.

75. Chiti, F., P. Webster, N. Taddei, A. Clark, M. Stefani, et al. 1999. Designing conditions for *in vitro*, formation of amyloid protofilaments and fibrils. *Proc. Natl. Acad. Sci. USA.* 96:3590–3594.

76. Krishnan, R., and S. L. Lindquist. 2005. Structural insights into a yeast prion illuminate nucleation and strain diversity. *Nature.* 435:765–772.

77. Moraitakis, G., and J. M. Goodfellow. 2003. Simulations of human lysozime: probing the conformations triggering amyloidosis. *Biophys. J.* 84:2149–2158.

78. Modler, A. J., K. Gast, G. Lutsch, and G. Damaschun. 2003. Assembly of amyloid protofibrils via critical oligomers. A novel pathway of amyloid formation. *J. Mol. Biol.* 325:135–148.

79. Serio, T. R., A. G. Cashikar, A. S. Kowal, G. J. Sawicki, J. J. Moleshi, et al. 2000. Nucleated conformational conversion and the replication of conformational information by a prion determinant. *Science.* 289: 1317–1321.

80. Jiang, Y., H. Li, L. Zhu, J. M. Zhou, and S. Perrett. 2004. Amyloid nucleation and hierarchical assembly of Ure2p fibrils. Role of asparagines/glutamine repeat and nonrepeat regions of the prion domains. *J. Biol. Chem.* 279:3361–3369.

81. Makin, O. S., and L. C. Serpell. 2005. X-ray diffraction studies of amyloid structure. *Methods Mol. Biol.* 299:67–80.

82. Sambashivan, S., M. R. Liu, M. R. Sawaya, M. Gingery, and D. Eisenberg. 2005. Amyloid-like fibrils of ribonuclease A with three-dimensional domain-swapped and native-like structures. *Nature.* 437:266–269.

83. Ranson, N., T. Stromer, L. Bousset, R. Melki, and R. C. Serpell. 2006. Insights into the architecture of the Ure2p yeats protein assemblies from helical twisted fibrils. *Protein Sci.* 15:2481–2487.

84. Hatters, D. M., C. A. MacRails, R. Daniels, W. S. Gosal, N. H. Thomson, et al. 2003. The circularization of amyloid fibrils formed by apolipoprotein C–II. *Biophys. J.* 85:3979–3990.

85. Lashuel, H. A., and P. T. Lansbury Jr. 2006. Are amyloid diseases caused by protein aggregates that mimic bacterial pore-forming toxins? *Q. Rev. Biophys.* 39:167–201.

86. Meehan, S., T. P. J. Knowles, A. J. Baldwin, J. F. Smith, A. M. Squires, et al. 2007. Characterization of amyloid fibril formation by small heat-shock chaperone proteins human αA-, αB- and R120G αB-crystallins. *J. Mol. Biol.* 372:470–484.

87. Kad, N. M., S. L. Myers, D. P. Smith, S. E. Radford, and N. H. Thomson. 2003. Hierarchical assembly of β2-microglobulin amyloid in vitro revealed by atomic force microscopy. *J. Mol. Biol.* 330:785–797.

88. Khurana, R., J. L. Jimenez, E. J. Nettleton, M. Bouchard, C. V. Robinson, et al. 2002. The protofilament structure of insulin amyloid fibrils. *Proc. Natl. Acad. Sci. USA.* 99:9196–9201.

89. Otzen, D. E., and M. Oliveberg. 2004. Transient formation of nanocrytalline structures during fibrillation of an Alzheimer-like peptide. *Protein Sci.* 13:1417–1421.

90. Grudzielanek, S., V. Smirnovas, and R. Winter. 2006. Solvation-assisted pressure tuning of insulin fibrillation: from novel aggregation pathways to biotechnological applications. *J. Mol. Biol.* 356:497–506.

91. Green, J. D., C. Goldsbury, J. Kistler, G. K. Cooper, and U. Aebi. 2004. Human amylin oligomer growth and fibril elongation define two distinct phases in amyloid formation. *J. Biol. Chem.* 279:12206–12212.

92. Chamberlain, A. K., C. E. MacPhee, J. Zurdo, L. A. Morozova-Roche, H. A. O. Hill, et al. 2000. Ultrastructural organization of amyloid fibrils by atomic force microscopy. *Biophys. J.* 79:3282–3293.

93. Goldsbury, C. S., S. Wirtz, S. A. Müller, S. Sunderji, P. Wicki, et al. 2000. Studies on the in vitro assembly of Aβa-40: implications for the search for Aβ fibril formation inhibitors. *J. Struct. Biol.* 130: 217–231.

94. Petkova, A. T., R. D. Leapman, Z. Guo, W. M. Yau, M. P. Mattson, et al. 2005. Self-propagating, molecular-level polymorphism in Alzheimer's β-amyloid fibrils. *Science.* 307:262–265.